Acta Crystallographica Section A
Foundations and Advances
ISSN 2053-2733

Received 23 December 2013
Accepted 28 February 2014

Atomic clusters and atomic surfaces in icosahedral quasicrystals[1]

Marianne Quiquandon,[a,b] Richard Portier[b] and Denis Gratias[a,b]*

[a]LEM UMR 104, CNRS–ONERA, 29 Avenue de la division Leclerc, F-92322 Chatillon Cedex, France, and [b]Institut de Recherche de Chimie Paris, UMR 8247, ENSCP, 11 rue Pierre et Marie Curie, F-75005 Paris, France. Correspondence e-mail: denis.gratias@onera.fr

This paper presents the basic tools commonly used to describe the atomic structures of quasicrystals with a specific focus on the icosahedral phases. After a brief recall of the main properties of quasiperiodic objects, two simple physical rules are discussed that lead one to eventually obtain a surprisingly small number of atomic structures as ideal quasiperiodic models for real quasicrystals. This is due to the fact that the atomic surfaces (ASs) used to describe all known icosahedral phases are located on high-symmetry special points in six-dimensional space. The first rule is *maximizing the density* using simple polyhedral ASs that leads to two possible sets of ASs according to the value of the six-dimensional lattice parameter A between 0.63 and 0.79 nm. The second rule is *maximizing the number of complete orbits of high symmetry* to construct as large as possible atomic clusters similar to those observed in complex intermetallic structures and approximant phases. The practical use of these two rules together is demonstrated on two typical examples of icosahedral phases, *i*-AlMnSi and *i*-CdRE (RE = Gd, Ho, Tm).

1. Introduction

Quasicrystals were first observed by D. Shechtman in April 1982 using electron microscopy on a rapidly solidified alloy of Al and Mn. The discovery was announced two years later (Shechtman *et al.*, 1984; Shechtman & Blech, 1985) together with a theoretical description developed independently by Levine & Steinhardt (1984) of a new kind of nonperiodic long-range-ordered solid they called *quasicrystals*.

These structures are solids – mostly metallic alloys – the diffraction patterns of which show sharp, well defined peaks that distribute in reciprocal space according to point symmetries inconsistent with three-dimensional periodicity. The wavevectors of the diffraction peaks can be unambiguously written as *linear integer combinations* of $n > 3$ basic vectors pointing on the vertices of a regular polyhedron of the same symmetry as the diffraction pattern, $\mathbf{q} = \sum_{i=1}^{n} n_i \mathbf{e}_i$, $n_i \in \mathbb{Z}$. This set of reflections forms a dense set of points called a $\mathbb{Z}$-module and was introduced to crystallography by Janner & Janssen (1977) as the basic concept in the description of incommensurate structures: both kinds of solids, quasicrystals and incommensurate phases, are quasiperiodic structures (see Esclangon, 1904; Bohr, 1924, 1925, 1926; Besicovitch, 1932).

[1] This article forms part of a special issue dedicated to mathematical crystallography, which will be published as a virtual special issue of the journal in 2014.

2. *N*-dimensional crystallography

A $\mathbb{Z}$-module in a space of dimension d can be viewed as the irrational projection of a n-dimensional lattice $n > d$ where n is the rank of the $\mathbb{Z}$-module.[2] The n-dimensional configurational space $\mathbf{E}^n$ can be decomposed in two orthogonal subspaces:

$$\mathbf{E}^n = \mathbf{E}_\parallel \oplus \mathbf{E}_\perp \tag{1}$$

where $\mathbf{E}_\parallel$ is the subspace of dimension d that represents the *physical space* and $\mathbf{E}_\perp$ the subspace of dimension $(n-d)$, complementary to $\mathbf{E}_\parallel$ and perpendicular to it, designated as *internal* space in Janner & Janssen (1977). This subspace $\mathbf{E}_\perp$ is best understood (see Elser, 1996) as an *order parameter space*. Here it will be designated as *perpendicular space*.

The relative orientations of $\mathbf{E}_\parallel$ and $\mathbf{E}_\perp$ in $\mathbf{E}^n$ are best described using orthogonal projectors. Let $\{\alpha\}$ be a d-dimensional orthonormal basis of $\mathbf{E}_\parallel$ and $\{\overline{\alpha}\}$ a $(n-d)$-dimensional orthonormal basis of $\mathbf{E}_\perp$, and let $\{i\}$ be an orthonormal basis of $\mathbf{E}^n$. Designating the scalar product between $|u\rangle$ and $|v\rangle$ as $\langle u|v\rangle$ (Dirac notations), we define the subspaces $\mathbf{E}_\parallel$ and $\mathbf{E}_\perp$ by the following matrices:

$$\widehat{\mathbf{M}}^{\parallel}_{\alpha,i} = \kappa\langle\alpha|i\rangle, \quad \widehat{\boldsymbol{\pi}}^{\parallel}_{i,j} = \kappa^2 \sum_{\alpha=1}^{d} \langle i|\alpha\rangle\langle\alpha|j\rangle, \tag{2}$$

[2] If $n = d$, the $\mathbb{Z}$-module is simply a d-dimensional lattice.

Table 1
Irreducible representations of the point group 235.

	$\hat{1}$	$(\hat{5}, \hat{5}^4)$	$(\hat{5}^2, \hat{5}^3)$	$\hat{2}$	$(\hat{3}, \hat{3}^2)$
A_1	1	1	1	1	1
Γ_3	3	τ	$1-\tau$	-1	0
$\Gamma_{\bar{3}}$	3	$1-\tau$	τ	-1	0
Γ_4	4	-1	-1	0	1
Γ_5	5	0	0	1	-1
Γ_6	6	1	1	-2	0

$$\widehat{\mathbf{M}}^{\perp}_{\overline{\alpha},i} = \kappa\langle\alpha|i\rangle, \quad \widehat{\boldsymbol{\pi}}^{\perp}_{i,j} = \kappa^2 \sum_{\overline{\alpha}=1}^{n-d} \langle i|\overline{\alpha}\rangle\langle\overline{\alpha}|j\rangle, \tag{3}$$

where

$$\kappa = \left(\sum_{i=1}^{n} |\langle\alpha|i\rangle|^2\right)^{-1/2} \tag{4}$$

is the normalization factor.

The $d \times n$ and $(n-d) \times n$ matrices $\widehat{\mathbf{M}}^{\parallel(\perp)}$ give the components of the projection in $\mathbf{E}_{\parallel}$ ($\mathbf{E}_{\perp}$) of a vector expressed in the internal bases $\{\alpha\}$ ($\{\overline{\alpha}\}$), whereas the $n \times n$ matrices $\widehat{\boldsymbol{\pi}}^{\parallel(\perp)}$ give these same components but expressed on the basis $\{i\}$ of $\mathbf{E}^n$.

Applying these rules to icosahedral quasicrystals leads one to choose $\mathbf{E}^6$ as the Euclidean space generated by the *six* vectors defined by the vertices of a regular icosahedron in $\mathbf{E}_{\parallel}$ and $\mathbf{E}_{\perp}$ as shown in Fig. 1.

Then, $\mathbf{E}_{\parallel}$ is a three-dimensional subspace belonging to the representation Γ_3 and $\mathbf{E}_{\perp}$ its orthogonal complement to six dimensions, belonging to the representation $\Gamma_{\bar{3}}$ of Table 1. Details of the geometry and indexing specific to the icosahedral phases can be found in Cahn *et al.* (1986).

2.1. *N*-dimensional description

Quasicrystalline structures are defined by:

(*a*) the rank n of the $\mathbb{Z}$-module (the dimension n of $\mathbf{E}^n$),

(*b*) the n-dimensional Bravais lattice Λ,

(*c*) the n-dimensional space group $\mathcal{G}$ that is the set of the hyperspace isometries g of the n-dimensional lattice that keep $\mathbf{E}_{\parallel}$ parallel to itself, *i.e.*

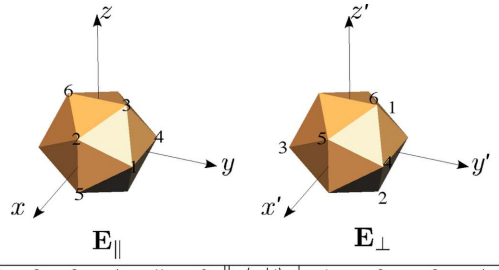

$\mathbf{E}_{\parallel}$ $\mathbf{E}_{\perp}$

$\langle\alpha\|i\rangle$	1	2	3	4	5	6	$\langle\bar{\alpha}\|i\rangle$	1	2	3	4	5	6
x	1	τ	0	-1	τ	0	x'	$-\tau$	1	0	τ	1	0
y	τ	0	1	τ	0	-1	y'	1	0	$-\tau$	1	0	τ
z	0	1	τ	0	-1	τ	z'	0	$-\tau$	1	0	τ	1

Figure 1
Orientations of the vertices of the basic icosahedron in $\mathbf{E}_{\parallel}$ and $\mathbf{E}_{\perp}$.

$$\mathcal{G} = \{\widehat{\mathbf{g}} \in \mathcal{N}(\Lambda);\ [\widehat{\mathbf{g}}, \widehat{\boldsymbol{\pi}}_{\parallel}] = \widehat{\mathbf{0}}\}, \tag{5}$$

(*d*) the set of atomic surfaces (ASs) – or acceptance domains – that are defined by their geometric shape in $\mathbf{E}_{\perp}$ and location in the n-dimensional unit cell and are associated with the various chemical species.

The ASs are described by a *finite* number of parameters with the exception of those concerning their geometric shapes that can *a priori* be infinite. Additional physical constraints (no unphysical short distances, local isomorphism, existence of matching rules and easy phason relaxation) are useful to reduce them to a finite number. Then, ASs are polygons (decagonal phases) or polyhedra (icosahedral phases) parallel to $\mathbf{E}_{\perp}$.

Density and stoichiometry are easily computed in this framework: if V_t is the total volume of the ASs in $\mathbf{E}_{\perp}$, the jth chemical species has concentration $c_j = \sum_{k=1}^{p} v_k^j / V_t$ where v_k^j are the volumes of the p ASs corresponding to the atomic species j.

2.2. Basic modelling

For icosahedral quasicrystals, the ASs are polyhedra in three-dimensional space parallel to $\mathbf{E}_{\perp}$. We describe them here as a *union of convex polyhedra* where most of them are simply described as a set of tetrahedra in the elementary sector attached to a given six-dimensional site. The complete polyhedron is obtained by applying the elements of the little group of the six-dimensional site to the generating tetrahedra. For example, the canonical triacontahedron (convex hull of the projection in $\mathbf{E}_{\perp}$ of the six-dimensional unit cell) centred at the origin (0, 0, 0, 0, 0, 0) is generated by applying the 120 symmetry elements of $m35$ to the tetrahedron $T_c = \{[0, 0, 0], [0, 0, 1+\tau], [0, 1, 1+\tau], [\tau, 0, 1+\tau]\}$, the vertices of which are the projections in $\mathbf{E}_{\perp}$ of the six-dimensional nodes, respectively, $a = (0, 0, 0, 0, 0, 0)$, $b = (0, \overline{1}, 1, 0, 1, 1)/2$, $c = (1, \overline{1}, 1, 1, 1, 1)/2$ and $d = (\overline{1}, \overline{1}, 1, 1, 1, 1)/2$. With no loss of generality, we *arbitrarily* give to this canonical triacontahedron in $\mathbf{E}_{\perp}$ the volume $V_t = \tau^3 = 1 + 2\tau$ to fix the length scale in $\mathbf{E}_{\perp}$.

All known icosahedral phases belong to either one of the two types of six-dimensional lattices, $P(1)$ and $F(2)$, defined as (see Cahn *et al.*, 1986): $P(1) = \{(n_1, n_2, n_3, n_4, n_5, n_6)\, n_i \in \mathbb{Z}\}$ and $F(2) = \{(n_1, n_2, n_3, n_4, n_5, n_6)\, n_i \in \mathbb{Z},\ \sum_i n_i = 0 \bmod 2\}$.

The diffraction experiments have shown that the major ASs of all presently known icosahedral phases are located at a few high-symmetry special points[3] of $m35$ in six dimensions that are:[4]

$$\begin{array}{cc} n = (0,0,0,0,0,0) & n' = (1,0,0,0,0,0) \\ bc = 1/2(\overline{1},1,1,1,1,\overline{1}) & bc' = 1/2(1,1,1,1,1,\overline{1}) \end{array}$$

where, for $P(1)$ structures, n', bc' are, of course, identical to, respectively, n and bc.

[3] Special points are positions in the unit cell with centred little groups, *i.e.* positions with no degree of freedom.

[4] Sometimes with the addition of small ASs located at the mid-edge $1/2(1, 0, 0, 0, 0, 0)$ that will not be considered here.

The first request for plausibly modelling the atomic structure of a quasicrystal is the density of the model: the ASs must be large enough to fit the experimental density. To have an order of magnitude, we consider that a standard metallic atom in a crystal occupies roughly 0.015 nm^3, the density d of nodes should be in the order of $d \simeq 66\ \text{nm}^{-3}$. Thus, using the previous length scaling in $\mathbf{E}_\perp$, we obtain the density of atom sites per nm^3 in real space as

$$dA^3 = \frac{\nu}{\kappa(\tau+1)} V_t \qquad (6)$$

where κ is the geometric normalization factor [equation (4)], A is the six-dimensional $P(1)$ lattice parameter expressed in nm, ν takes values 1/2, 1 or 2 for, respectively, $F(2)$, $P(1)$ and $I(1)$ six-dimensional lattice types, and V_t is the total volume of the ASs in the six-dimensional unit cell. Thus, the total volume of the ASs is roughly $66A^3/\nu$ per primitive unit cell.

For example, one finds $V_t \simeq 16.6$ for the F-type phase of i-AlCuFe with parameter $A = 0.63146$ nm and $V_t \simeq 17.5$ for i-AlPdMn of parameter $A = 0.645$ nm. For a larger parameter, like i-CdYb primitive structures with $A = 0.75$ nm, the total AS volume jumps to $V_t \simeq 27.8$. This shows that the ASs used for these last $P(1)$ structures are significantly larger than those used for the latter $F(2)$ structures. Fig. 2 shows the ASs chosen to model the icosahedral structures having small six-dimensional parameters around 0.65 nm. They are determined in noting that short atomic distances are observed along the fivefold and threefold directions according to:

(a) In the fivefold direction

$$-(n-n') : (\bar{2},1,1,1,1,\bar{1})\,[(18-11\tau)^{1/2},\ 0.1669\,A]$$
$$-(n'-bc) : (1,1,\bar{3},1,\bar{1},1)/2[(7-4\tau)^{1/2}, 0.2701A].$$

(b) In the threefold direction

$$-(n-bc') : (\bar{3},1,1,3,3,1)/2\,[(15-9\tau)^{1/2}, 0.2459A].$$

Imposing the ASs located at these various locations to have no intersections once projected in $\mathbf{E}_\perp$, we obtain the shapes of the ASs given in Fig. 2, hereafter called model A. The total volume per $P(1)$ unit cell for the $F(2)$ is $(11+14\tau)/2 \simeq 16.826$ and for the $P(1)$ set $(77+106\tau)/15 \simeq 16.567$, in excellent agreement with what is expected from equation (6).

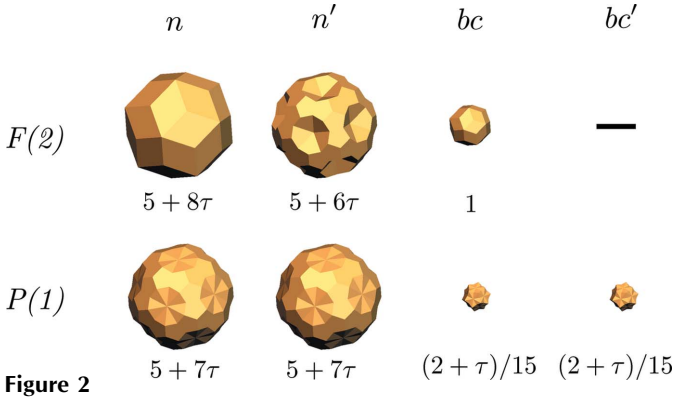

Figure 2
The set A of global ASs used to model icosahedral structures with a small six-dimensional parameter around 0.65 nm. The shape of the AS located at the node $n(n')$ for the $P(1)$ structure is due to Henley (1986). This $P(1)$ set can be used for the $F(2)$ structure by assigning different atomic species between n and n', and between bc and bc'. The volumes of the ASs are, for $F(2)$: $V_n = 5+8\tau$, $V_{n'} = 5+6\tau$, $V_{bc} = 1$, $V_{bc'} = 0$; for $P(1)$: $V_{n(n')} = 5+7\tau$, $V_{bc(bc')} = (2+\tau)/15$.

Now, for A parameters larger than 0.74 nm, the distance $n'-bc$ along the fivefold direction becomes acceptable (0.2 nm). This relaxes one constraint and leads to the new set of ASs shown in Fig. 3, hereafter called model B. Here, the total volume per $P(1)$ unit cell for the $F(2)$ is $(10+9\tau) \simeq 24.562$ and for the $P(1)$ set $(103+164\tau)/15 \simeq 24.557$, values that are a little smaller but in rough agreement with the value given by equation (6).

Both sets A and B form a nicely connected network of ASs closed at short distances as shown in Fig. 4. The $n-n$ [even connections in $F(2)$ structures] connections are along the twofold direction $(\bar{1},\bar{1},2,0,2,0)$ of jump distance $0.284A$, and $n-n'$ [odd connections in $F(2)$ structures] connections are along the fivefold direction $(\bar{2},1,1,1,1,\bar{1})$ of jump distance

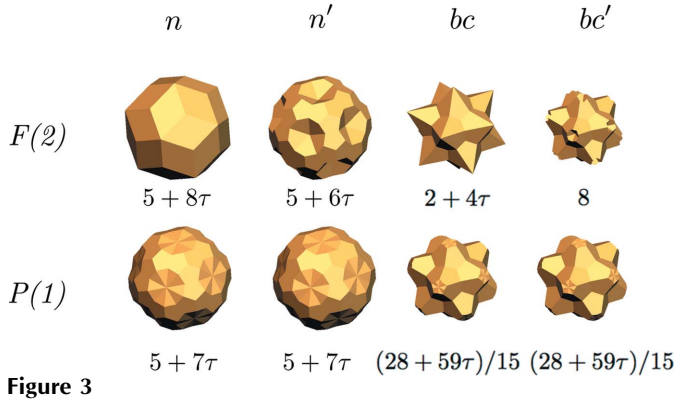

Figure 3
The set B of global ASs used to model icosahedral structures with a large six-dimensional parameter above 0.7 nm. This set differs from set A in the global ASs located on bc. Here, too, the $P(1)$ set can be used for modelling the $F(2)$ structure. The volumes of the ASs are, for $F(2)$: $V_n = 5+8\tau$, $V_{n'} = 5+6\tau$, $V_{bc} = 2+4\tau$, $V_{bc'} = 8$; for $P(1)$: $V_{n(n')} = 5+7\tau$, $V_{bc(bc')} = (28+59\tau)/15$.

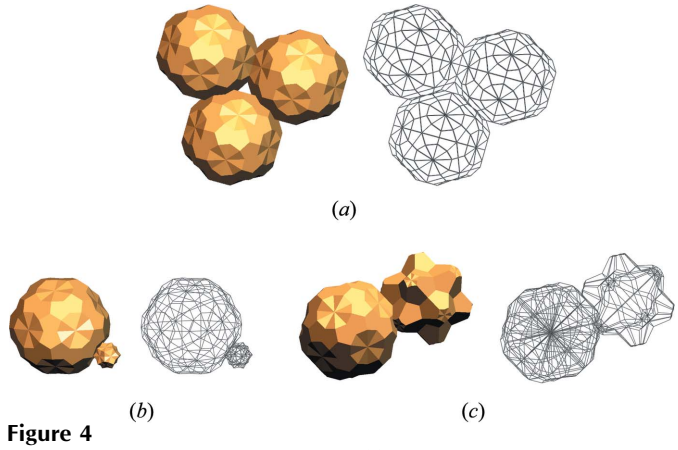

Figure 4
Connections between ASs for the $P(1)$ models A and B: (a) n sites connect together according to either the fivefold direction by odd connections at $\kappa(18-11\tau)^{1/2}A = 0.167A$, or the 2f direction through even connections at $\kappa(20-12\tau)^{1/2}A \simeq 0.284A$ directions; (b) for the A model, the connections $n-bc$ occur all along the fivefold direction at $\kappa(7-4\tau)^{1/2} = 0.270A$. ($c$) Finally, for the B model, the connection $n-bc$ occurs along the threefold direction at $\kappa(15-9\tau)^{1/2} = 0.246A$.

0.167A, whereas $n-bc$ occurs along the fivefold direction $(\bar{3},1,1,1,1,\bar{1})/2$ of jump distance 0.270A and, additionally for model B, there is a connection along the threefold direction $(\bar{1},\bar{1},\bar{1},3,3,3)/2$ with a jump distance 0.246A. These four connection types define the set of thermodynamically stable phasons generated in these models.

3. Local atomic configurations

Beyond the density of the structural models, it is important to characterize their local atomic configurations. Hence, quasicrystals described by ASs aligned along $\mathbf{E}_\perp$ such that Λ projects as a uniformly dense set of points in $\mathbf{E}_\perp$ have the two following basic properties:

(i) The *uniformity property* states that any finite packing of tiles which appears in a given quasiperiodic tiling appears infinitely many times in the same tiling with a well defined frequency; for any given *finite* radius r, there exists only a *finite* number of different atomic configurations.

(ii) The *local isomorphism property* asserts that any finite packing of tiles which appears in a given quasiperiodic tiling in $\mathbf{E}_\parallel$ appears with the *same* frequency in all tilings generated by *any other* cuts parallel to $\mathbf{E}_\parallel$.

Because of these two theorems, the local structure of models with flat atomic surfaces can be exhaustively described by a list of *all* possible local atomic configurations within a ball of radius r, each with its own frequency. The larger the radius r is, the finer is the crystallographic description.

It is best to analyse these atomic local configurations directly in $\mathbf{E}_\perp$ where all the geometrical environments have a finite-size image that can be calculated exactly. The natural way of achieving this is the cell (Oguey *et al.*, 1988) or 'Klötze' decomposition (Kramer, 1988; Arnol'd, 1988) that is based on the simple idea that *two actually present atoms in the structure are issued from two atomic surfaces, the projection in* $\mathbf{E}_\perp$ *of which has a non-empty intersection* (see Fig. 5). Thus, studying how atomic surfaces projected in $\mathbf{E}_\perp$ intersect each other suffices to determine what kind of clusters are present in the real structure and their frequencies are proportional to their intersection volume in $\mathbf{E}_\perp$.

Let x_0 and x_1 be two sites of the structures generated by T_0 and T_1 atomic surfaces located at two hyperlattice nodes, say λ_0 and λ_1. We have $x_0=\widehat{\pi}_\parallel\lambda_0=\lambda_{0\parallel}$ and $x_1=\widehat{\pi}_\parallel\lambda_1=\lambda_{1\parallel}$. The two points are connected by the vector x_1-x_0 in $\mathbf{E}_\parallel$ corresponding to the hyperlattice node $t=\lambda_1-\lambda_0$ that has perpendicular component $t_\perp=\widehat{\pi}_\perp t$. Thus the two points x_0 and x_1 being *simultaneously* present in the structure, the two atomic surfaces T_0 and T_1 displaced by $t_\perp$ in $\mathbf{E}_\perp$, must have a non-zero intersection. All the pairs of the type (x_0,x_1) are thus generated by the subset of atomic surfaces defined by $T_0\cap T_1(t_\perp)$. This is the existence domain for the pair (x_0,x_1):

$$T(x_0,\ x_1=x_0+t_\parallel)=T_0\cap T_1(t_\perp). \tag{7}$$

The *relative* density (number of x_0 points that are attached to such a pair divided by the total number of x_0 points) is given by

$$\rho(T_0,t_\parallel)=\frac{|T_0\cap T_1(t_\perp)|}{|T_0|} \tag{8}$$

where $|T_i|$ designates the volume of the polyhedron T_i.

More generally, if we consider a set containing a finite number N of points of the structure, say $x_0,x_1,\ldots,x_N$ located at $t_\parallel^1,t_\parallel^2,\ldots,t_\parallel^N$ with x_0 taken as the origin, the existence domain of this set is given by $T_0\cap T_1(t_\perp^1)\cap T_2(t_\perp^2)\cap\ldots\cap T_N(t_\perp^N)$ with the relative density

$$\rho(T_0,t_\parallel^1,\ldots,t_\parallel^N)=\frac{|T_0\cap T_1(t_\perp^1)\cap\ldots\cap T_N(t_\perp^N)|}{|T_0|}. \tag{9}$$

As an example, Fig. 6 shows the basic vertex decomposition in the elementary sector of the standard three-dimensional Penrose canonical tiling obtained by the intersections of the canonical triacontahedron onto itself under the fivefold translation $(1,0,0,0,0,0)$. Superimposing all 12 equivalent translated triacontahedra on top of the central one leads to a decomposition into nine different cells, corresponding to the nine different vertex configurations to $(1,0,0,0,0,0)$ neighbours.

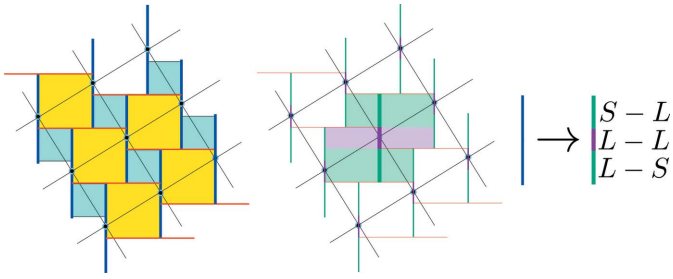

Figure 5
Principle of the cell decomposition on the one-dimensional Fibonacci sequence in a two-dimensional space: $\mathbf{E}_\parallel$ is any horizontal line and $\mathbf{E}_\perp$ any vertical one. The ASs (vertical segments in blue) define two kinds of two-dimensional area. Each time $\mathbf{E}_\parallel$ passes through a blue square it generates a short-distance S pair of sites, and each time it passes through a yellow square it generates a long-distance L pair of sites. Thus the initial AS can be decomposed into three cells (segments): the two green segments collect all points that have an S bound on one side and an L on the other, and the purple segment that generates sites that have L bounds on both sides.

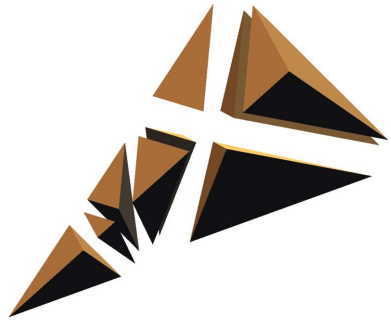

Figure 6
By intersection with the 12 copies of itself along the fivefold direction $(1,0,0,0,0,0)$, the canonical triacontahedron decomposes into nine cells that correspond to the different vertex configurations. Cells are represented here inside the elementary tetrahedron expanded for showing the various cells. Each configuration appears in the three-dimensional tiling with a frequency proportional to the volume of the corresponding cell.

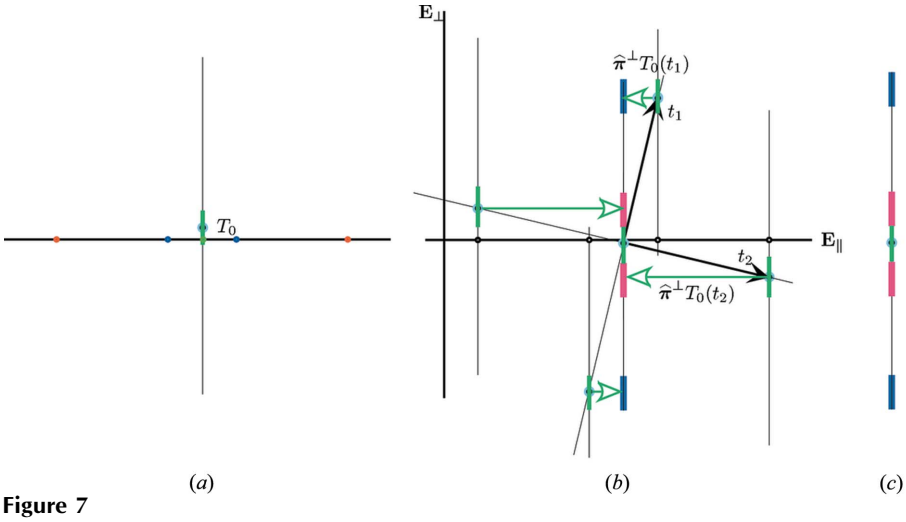

Figure 7
One-dimensional example of constructing (*b*) the proper ASs (*c*) that generate the atomic cluster with a green atom at the centre generated by T_0 (*a*), blue atoms at distance $t_{1,\parallel}$ and red atoms at distance $t_{2,\parallel}$. See text for further details.

Table 2
Characteristics of the main ASs shown in Fig. 8 defining the icosahedral orbits around the origin *n*.

ASs with bold numbers intersect the basic ASs of models *A* or *B*. ASs with the same superscript form a triacontahedron (2 + 7, 8 + 14 and 12 + 15).

AS No.	Located at	Six-dimensional translation $[N, M] : (n_1, n_2, \ldots, n_6)$	Multiplicity ν	Radius in *A* unit
1	*n*	[20,12]:(0,2,−1,0,−2,−1)	30	0.284
2*	*n*′	[6,−3]:(1,0,0,−1,−1,0)	20	0.398
3	*bc*	[15,−9]:(−3,1,1,3,3,1)/2	20	0.246
4	*bc*′	[7,−4]:(1,1,−3,1,−1,1)/2	12	0.270
5	*n*	[4,0]:(0,1,0,0,−1,0)	30	0.744
6	*n*′	[8,−4]:(0,−1,1,0,1,1)	30	0.459
7*	*bc*	[3,−1]:(1,1,−1,1,−1,1)/2	12	0.437
8†	*bc*′	[3,0]:(−1,1,1,1,1,1)/2	20	0.644
9	*n*	[12,−4]:(1,1,−1,1,−1,1)	12	0.874
10	*n*′	[14,−7]:(1,0,−1,1,0,2)	60	0.608
11	*bc*	[7,−1]:(1,−1,1,1,1,3)/2	60	0.862
12‡	*bc*′	[3,4]:(1,1,1,1,−1,1)/2	12	1.144
13	*n*	[12,−4]:(−1,0,2,0,1,0)	60	0.874
14†	*n*′	[2,1]:(1,0,0,0,0,0)	12	0.707
15‡	*bc*	[3,3]:(1,1,1,−1,−1,1)/2	20	1.042
16	*bc*′	[7,0]: (1,−1,−3,1,1,1)/2	60	0.984

3.1. Atomic clusters

Our second guide to the structural determination of icosahedral quasicrystals is the fact that their known approximant phases all exhibit typical high-symmetry atomic clusters (ACs) that are expected to be also present in the quasicrystalline parent phase and which have been discussed in particular by Steurer (2006), Henley *et al.* (2006), and studied in the six-dimensional context by Steurer & Deloudi (2012). Our present goal is to reshape the previously defined *A* and *B* basic sets of ASs in order to generate *as large as possible* ACs with the highest possible symmetry.

We define an atomic cluster as a set of atomic positions characterized by the fact that *if any one of the atoms of the AC is present in the structure then all others of the AC are also present*. Let T_0 be the AS, located at some high-symmetry special point of the hyperlattice, that generates the centres of the ACs; each other point of the AC covers a domain that is the exact[5] copy of T_0, and is entirely contained in the atomic surfaces. Thus, the ASs must contain the union of these copies, each corresponding to one point of the AC. The global AS must then have the high symmetry of the cluster and therefore be attached to a high-symmetry special point of the hyperlattice.

If the AC is made of *N* orbits, each orbit *j* of M_j surrounding atoms characterized by translations $\widehat{\pi}_\parallel t_j^k$:

$$\mathrm{AC} = \cup_{j=1}^{N} \cup_{k=1}^{M_j} \widehat{\pi}_\parallel t_j^k, \qquad (10)$$

the global AS, say $\mathrm{AS_{AC}}$, is obtained by the union of all T_0's located in $\mathbf{E}_\perp$ at $\widehat{\pi}_\perp t_j^k$ sites in six dimensions:

$$\mathrm{AS_{AC}} = \cup_{j=1}^{N} \cup_{k=1}^{M_j} T_0(\widehat{\pi}_\perp t_j^k). \qquad (11)$$

The construction algorithm of $\mathrm{AS_{AC}}$ is therefore the following:

(*a*) starting from T_0, that is the AS generating the centre, we copy it on all six-dimensional nodes t_j^k corresponding to the atoms of the cluster in $\mathbf{E}_\parallel$;

(*b*) we then project these copies on $\mathbf{E}_\perp$ to obtain the set [equation (11)] of $T_0(\widehat{\pi}_\perp t_j^k)$; this set forms the searched $\mathrm{AS_{AC}}$ on the initial node;

(*c*) the $\mathrm{AS_{AC}}$ is finally copied on all equivalent six-dimensional nodes.

Let us illustrate the process by a simple one-dimensional example shown in Fig. 7. We search for the AS that generates a set of ACs made of a green atom centre generated by T_0 (Fig. 7*a*), two blue atoms at a distance $\widehat{\pi}_\parallel t_1$ and two red atoms at a distance $\widehat{\pi}_\parallel t_2$. We copy T_0 at t_1 and t_2 and their equivalent nodes by symmetry (here simply the inversion $-t_1$ and $-t_2$) and then project these copies on $\mathbf{E}_\perp$ (Fig. 7*b*), *i.e.* $T_0(\widehat{\pi}_\perp t_1)$, $T_0(-\widehat{\pi}_\perp t_1)$ and $T_0(\widehat{\pi}_\perp t_2)$, $T_0(-(\widehat{\pi}_\perp t_2)$. This eventually defines a global AS made of five cells in $\mathbf{E}_\perp$: the central green segment, two adjacent red and two blue in the periphery as shown in Fig. 7(*c*).

3.2. Maximal density and largest high-symmetry atomic clusters

The choice of T_0 is *a priori* arbitrary but an optimized choice is obtained when $\mathrm{AS_{AC}}$ has the largest possible volume, *i.e.* when the cells $T_0(\widehat{\pi}_\perp t_j^k)$ in equation (11) have the smallest intersections.

For icosahedral phases, the choice of the Henley's truncated triacontahedron (Henley, 1986) used to model *P*(1) structures, shown in Figs. 2 and 3 at the node *n* and scaled by τ^{-2} as generator T_0, is extremely efficient for ensuring a maximum covering on *n* and *bc*. Fig. 8 shows the few first ASs that

[5] Else there would be missing atoms of the AC around certain centres, or, on the contrary, missing centres for some ACs.

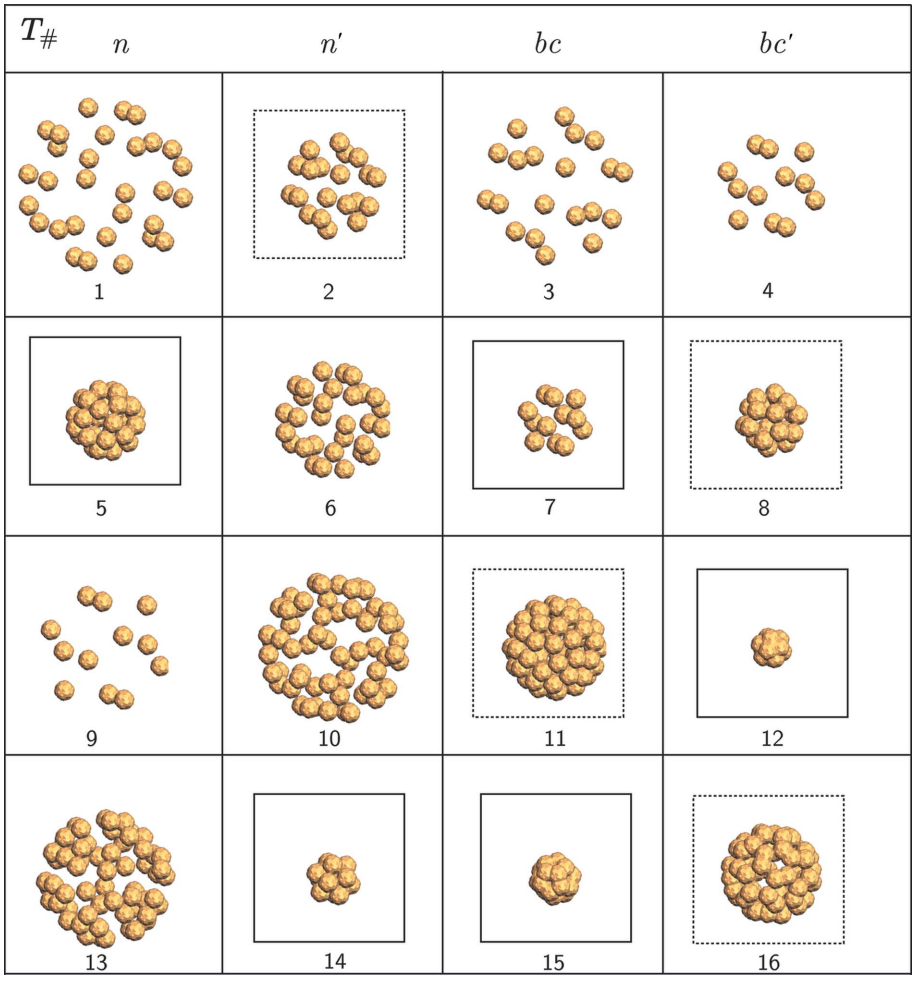

Figure 8
ASs attached to special points n, n', bc and bc' [merge n and n', bc and bc' for $P(1)$ structures] generating the orbits of atomic clusters of radius smaller than the six-dimensional lattice parameter A described in Table 2. The ASs contained in the global ASs of model B are enclosed in solid-line rectangles; those enclosed in dashed-line rectangles are partially contained in the global ASs.

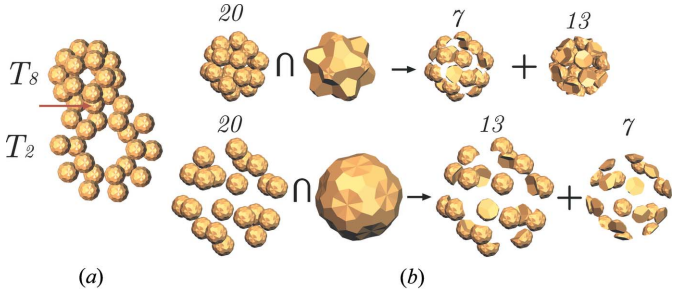

Figure 9
(*a*) ASs T_2 and T_8 intersect according to an exact T_0 subcell (red arrow) once displaced from each other by $(1, 1, 1, \bar{3}, \bar{3}, \bar{3})/2$. (*b*) The various intersections of T_2 and T_8 with the global ASs of model B show that keeping one complete orbit in a model requires removing the other from the model. This is achieved at constant total volume.

generate high-symmetry atomic orbits defined in Table 2 using this generator.

When the union of the T_0 fills all the global ASs of the model, then the corresponding cluster covers all the atoms of the model. This is a very special case: besides clusters of one point that cover obviously any structural model, edges of many tilings (two-dimensional and three-dimensional Penrose tiling, Amman–Beenker tiling) provide covering clusters of two points. In all other known cases, except the fascinating decagonal covering discovered by Gummelt (1996), atomic clusters do not cover the entire structure of the quasicrystal, meaning that real quasicrystals cannot be described by the atomic clusters only, in the sense that there are always remaining atoms that do not belong to the clusters.

The ASs that intersect or are inside the basic global ASs of models A or B are noted in bold on the left column of Table 2. In Fig. 8, the ASs T_1, T_3, T_4, T_6, T_9, T_{10} and T_{13} are largely outside the ASs of the models A and B. They are therefore most likely not to be used in standard modelling except for very large six-dimensional lattice parameters. On the contrary, the ASs that are most plausible in modelling the icosahedral phases are T_5, T_7, T_{12}, T_{14} and T_{15} since they are inside the global ASs. Finally, the ASs T_2 and T_8, that generate two homothetic dodecahedra in the τ ratio, intersect the basic global ASs but do have parts outside them.[6] Thus, using either of these two orbits in the modelling requires reshaping the large ASs to avoid the creation of atoms at too short a distance from each other. This is easily achieved by noticing that T_2 and T_8 share one exact T_0 when displaced by the $n - bc$ translation $(1, 1, 1, \bar{3}, \bar{3}, \bar{3})/2$ as shown in Fig. 9(*a*) (red arrow). Hence, keeping one of these two ASs in the modelling simply requires one to remove the latter from the global ASs either n or bc as shown in Fig. 9(*b*). If the full small dodecahedron is retained in the model corresponding to the whole T_2 of volume $20|T_0|$, then the global AS at n is increased by $13|T_0|$ but T_8, also of volume $20|T_0|$, is removed, thus reducing the global AS at bc by $13|T_0|$. On the contrary, if the large dodecahedron is retained in the model, corresponding to T_8, then the bc is increased by $7|T_0|$, but T_2 is removed thus reducing n by $7|T_0|$. Both cases are different models having the very same density. This is shown in Fig. 10.

Model (*a*) is the initial B model defined by maximizing the density of the structure [total volume $(103 + 164\tau)/15 \simeq 24.55\_7$]. Since it contains the ASs T_5, T_7 and T_{14}, the model generates around the node sites high-symmetry orbits of a small icosahedron (T_7), an icosidodecahedron (T_5), a large icosahedron (T_{14}), plus a partial small dodecahedron of 7 to 20

[6] The remaining ASs T_{11} and T_{16} will not be discussed here.

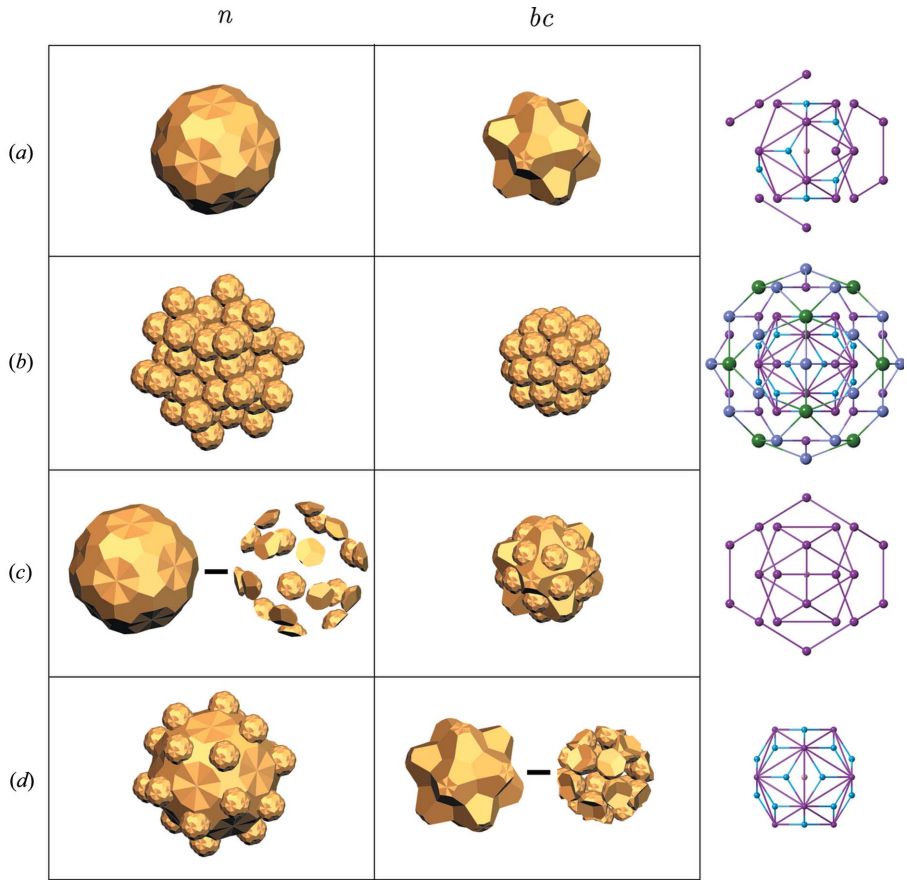

Figure 10
(*a*) Set *B* and corresponding AC inner shells of two incomplete dodecahedra corresponding to T_2 and T_8; (*b*) set of orbits of Table 2 intersecting the set *B*; this generates the maximum possible cluster including short distances between some atoms; (*c*) redistribution generating two complete orbits: an icosahedron and a complete large dodecahedron; (*d*) another distribution generating a complete icosahedron and a complete small dodecahedron. Structures generated by models (*a*), (*c*) and (*d*) have exactly the same density.

atoms (T_2) and another partial dodecahedron τ times larger of 13 to 20 atoms (T_8). These atomic clusters are encapsulated in large triacontahedra generated by T_{12} (icosahedra) and T_{15} (dodecahedra) forming the external shells of connections between two (by sharing vertices of the dodecahedra) and three (by sharing vertices of the icosahedra) clusters.

Model (*b*) is the model that maximizes the number of high-symmetry orbits irrespective of atoms possibly located at too short a distance from each other. It contains all previous complete orbits including those coming from ASs T_2 and T_8. These are the ASs proposed by Takakura *et al.* (2004) for modelling the atomic clusters of *i*-CdYb quasicrystals.[7] This model is very appealing but it generates atoms at short distances with a density that is still much too low [total volume $94(-37+23\tau) \simeq 20.189$], roughly 82.2% of model (*a*) because it generates only the atoms of the ACs. A remarkable fact is that this set of ASs built with T_2, T_3, T_{14} and T_0 at *n*, and T_6, T_5 at *bc* is the largest possible set of *non-overlapping* T_0 intersecting the global set *B*. Thus, the atomic cluster drawn for model (*b*) of Fig. 10 is the *largest possible cluster generated by* T_0 *in which each atom belongs to one and only one cluster*. It is made of a small inner triacontahedron generated by T_2 (dodecahedron) + T_7 (icosahedron), then a τ times larger triacontahedron generated by T_8 (dodecahedron) + T_{14} (icosahedron) and finally a large icosidodecahedron generated by T_5. All atomic clusters identified so far in real icosahedral phases are a subset of this general ideal cluster and for all real structures, T_{14} – generating a nicely connected set of icosahedra – is the privileged cell for the chemical ordering of the transition metal (Mn, Fe) or rare earth (Yb, Gd, ...).

Models (*c*) and (*d*) are two ways of increasing the number of high-symmetry orbits while keeping a constant density. The first one (*c*) consists of completing the large dodecahedron by using the complete orbit from AS T_8 on the *bc* and thus removing the corresponding fraction on *n*; the last one (*d*) consists of keeping the complete orbit of T_2 on the node and removing the corresponding part on the *bc* in order to generate a complete small internal triacontahedron. In model (*a*), only 47.2% of the atoms belong to a high-symmetry cluster, whereas, of course, this is 100% for model (*b*) and 64.7% for models (*c*) and (*d*). These last two models are therefore a good compromise for generating large high-symmetry atomic clusters together with an acceptable density.

4. Examples

We shall now illustrate, with two examples, the use of these geometric tools to construct simple ideal models of icosahedral phases that would be used as initial models for structure refinement or as plausible acceptable models for discussing and understanding some physical properties of those materials.

4.1. The case of *i*-AlMnSi

The alloy *i*-AlMnSi was discovered immediately after the original Shechtman alloy in the Al–Mn system. It is obtained by rapid solidification of a mother alloy of composition $Al_{73}Mn_{21}Si_6$. It has a primitive six-dimensional lattice with six-dimensional parameter $A = 0.6497$ nm and a volumic mass around $\rho = 3.62$ g cm^{-3}. On annealing above 973 K, the alloy transforms into crystalline β phase plus traces of aluminium.

[7] In their notations, *bc* and *n* are inverse from ours; our notations, however, are consistent with all the previous descriptions of icosahedral phases.

Beyond this relatively good quality, this alloy presents a cubic phase noted α-AlMnSi close to the composition $Al_{72.5}Mn_{17.4}Si_{10.1}$ of space group $Pm\overline{3}$, almost $Im\overline{3}$ with lattice parameter $A = 1.268$ nm (Cooper & Robinson, 1966). This cubic phase is the first cubic approximant[8] of the icosahedral phase that is expected to be $Im\overline{3}$ with lattice parameter $A = 1.265$ nm.

The α phase is principally made of two (almost) identical Mackay clusters centred on $(0, 0, 0)$ and $(1, 1, 1)/2$. These two clusters have an empty centre and are built with three orbits: a small icosahedron of average radius 0.245 nm filled with Al, an almost twice larger icosahedron of Mn of average radius 0.478 nm and an icosidodecahedron of Al of average radius 0.475 nm.

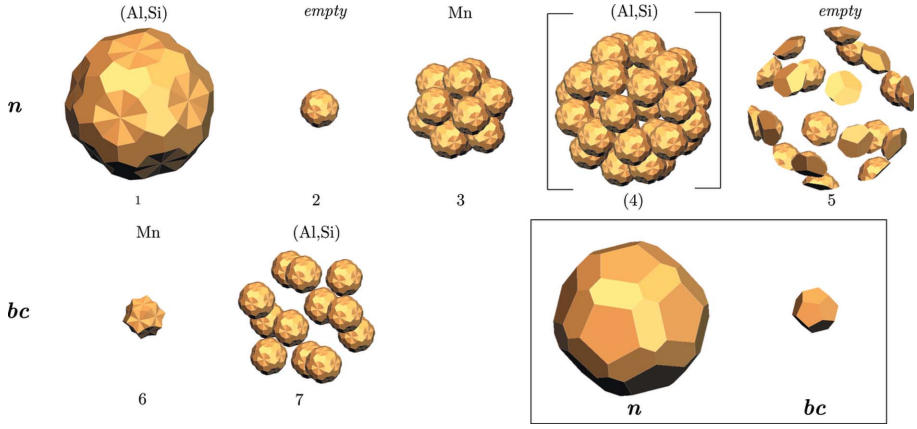

Figure 11
The simplest model of *i*-AlMnSi that generates atomic clusters reassembling the Mackay clusters observed on the α approximant structure. The volumes of the ASs are $V_1 = 5 + 7\tau$, $V_2 = -37 + 23\tau$, $V_3 = 12V_2$, $V_4 = 30V_2$, $V_5 = 7V_2$, $V_6 = (2 + \tau)/15$, $V_7 = 12V_2$. In the inset are the main atomic surfaces at *n* and *bc* of the initial model of Duneau & Oguey (that are replaced in our model by AS 1 and 6).

After first six-dimensional modelling using spherical atomic surfaces (see Cahn *et al.*, 1988; Gratias *et al.*, 1987), a very interesting six-dimensional model has been proposed by Duneau & Oguey (1989) using the truncated triacontahedron at *n* and the small dodecahedron at *bc* seen in the inset of Fig. 11.

The construction of the present six-dimensional model follows the one proposed by Duneau & Oguey (1989) but uses here the optimized ASs based on the Henley polyhedron. Because of the value of the six-dimensional parameter $A = 0.6497$ nm, we choose model *A* to construct the model shown in Fig. 11. In this figure AS 1 on *n* is first filled with a mixture of Al and Si. To generate the Mackay clusters similar to those of the α phase we first make the centres of the nodes empty by removing the small T_0 (AS 2) from AS 1. We then use the subcell T_{14} of Fig. 8 to generate the Mn large icosahedron (AS 3) filled with Mn atoms. Since the AS T_5 of Fig. 8 generating the icosidodecahedron of (Al,Si) is entirely contained in the large surface located at *n*, we do not need to add anything to the model [the AS 4 in Fig. 11 is drawn just for explicitly recalling the presence of the icosidodecahedron of (Al,Si) in the structure]. The last task is the construction of the cell generating the inner (Al,Si) icosahedron: this is achieved using the AS T_7 of Fig. 8 (AS 7 in Fig. 11) filled with (Al,Si) on *bc*. Because, as we have previously shown, this AS extends outside the global AS at *bc*, we have to remove the part of the AS at *n* that would generate atoms too close from this icosahedron; this is achieved by removing T_2 (the AS 5 from the large AS 1 of Fig. 11). Finally, we fill the small AS 6 at *bc* with Mn atoms.

The model has a total primitive volume $V_t = 5 + 7\tau + 4(-37 + 23\tau) + (2 + \tau)/15 = (-2143 + 1486\tau)/15 \simeq 17.426_5$ with a theoretical density $\rho = 3.42$ g cm^{-3} associated with the composition $(Al,Si)_{83.83}Mn_{16.17}$. Compared with the experimental composition of $(Al_{73}Si_6)Mn_{21}$, we observe that we must replace Al in the model by an average atom $\overline{Al} = (73Al + 5Mn + 6Si)$ leading thus to the proper stoichiometry and a volumic mass of 3.59 g cm^{-3}, close to the experimentally measured density. The atoms belonging to the Mackay clusters (see Fig. 12) correspond to a total volume of $54(-37 + 23\tau)$ and thus represent a fraction of $54(-37 + 23\tau)/V_t \simeq 0.665548$, *i.e.* roughly 2/3 of the total number of atoms. This is large enough for the Mackay clusters to qualify as being the typical atomic clusters in that structure but it is clearly not enough to reduce the structure to a simple aggregation of Mackay clusters. The resulting icosahedral

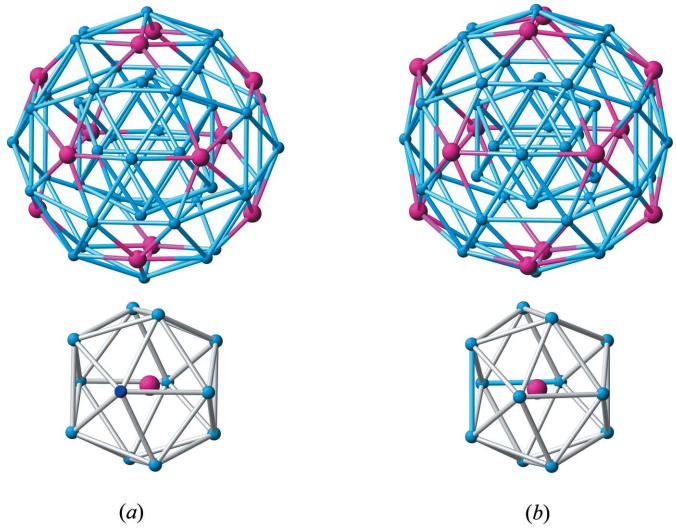

Figure 12
Top: comparison between the Mackay clusters (*a*) as generated by the icosahedral model, (*b*) as determined in the cubic α phase. Bottom: the neighbourhood of the Mn atoms in (*a*) the icosahedral model and (*b*) the α phase: both have a deformed icosahedron of aluminium, the strongest deformation being observed for the icosahedral model.

[8] In the present context, an approximant structure is a periodic structure obtained from parent quasicrystals but the irrationality is replaced by a rational approximation; in the present case, the golden mean τ is replaced by the rational fraction 1/1.

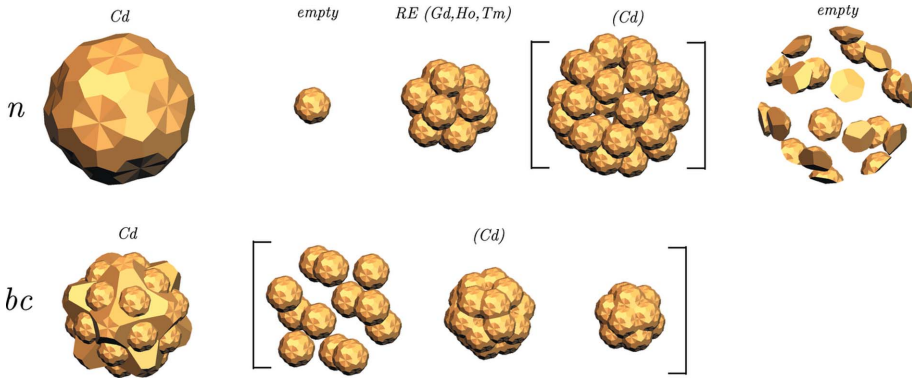

Figure 13
Simple model for the newly discovered *i*-$Cd_{88.5}RE_{11.5}$ (RE = Gd, Ho, Tm) primitive icosahedral phase. This model contains high-symmetry atomic clusters made of an inner icosahedron (that has to be changed into a highly disordered central tetrahedron), then a dodecahedron, the icosahedron of RE atoms, a large icosidodecahedron and finally an external triacontahedron linked to two or three other identical clusters.

Table 3
Comparison of the Mackay clusters of the α phase of lattice parameter $A_\alpha = 1.268$ nm with those in the present icosahedral model of theoretical lattice parameter $A_\alpha = 1.265$ nm.

The radii of the orbits of the Mackay clusters are given in nm. The distances between two closest Mn atoms are $d = 0.483$ nm in the icosahedral QC model and in the α phase $d = 0.512$ for M and $d = 0.506$ for M'.

	Model QC	$\alpha(M/M')$	β
Icosahedron Al	0.284	0.242/0.246	0.86
Icosahedron Mn	0.459	0.486/0.473	1.045
Icosidodecahedron Al	0.483	(0.472, 0.461)/(0.474, 0.479)	0.971

structure is constructed on the two $\mathbb{Z}$-modules centred on n and bc sites in $\mathbf{E}_\parallel$. The Mn atoms distribute on the vertices of a network of large icosahedra linked by octahedra along the 3f directions.

This model is of course an idealized structure that deserves further significant refinements. In particular, the Mackay clusters determined by standard crystallography in the α phase compared with those generated by the model are slightly different as shown in Fig. 12. The correction factors (see Table 3) for the orbit's radii on the Mackays between model and average values measured from the α phase are $\bar{r}_\alpha = \beta r_{QC}$ with $\beta = 0.86$ for the inner icosahedron of Al, $\beta = 1.045$ for the outer icosahedron of Mn and $\beta = 0.971$ for the external icosidodecahedron of Al as shown in Fig. 12.

4.2. The case of *i*-CdRE (RE = Gd, Ho, Tm)

The discovery of the *i*-$Cd_{85}Yb_{15}$ icosahedral phase by Tsai *et al.* (2000) has opened intense new structural studies on binary primitive icosahedral phases with a large six-dimensional lattice parameter (Takakura *et al.*, 2004). In particular, the *i*-CdRE (RE = Gd, Ho, Tm) family of composition close to the *i*-$Cd_{89}RE_{11}$ type presents a six-dimensional lattice parameter of $A = 0.7972$ nm for RE = Gd with interesting magnetic properties (Goldman *et al.*, 2013).

The main structural information has been given by Takakura *et al.* (2004) using a six-dimensional description with the ASs of Fig. 8, T_2, T_5, T_{14} on the node n, and T_7 and T_8 on the site bc (see Table 2). These ASs, regrouped in Fig. 10(*b*), generate a high-symmetry atomic cluster containing the maximum number of orbits (see Fig. 10*b*, right column) as described in the previous section. Adding ASs T_{12} and T_{15} of Fig. 8 (Table 2) to the model generates the outer triacontahedron that ensures the connections between clusters. This addition, however, is far from being enough to describe the entire structure. The main question at that level of course is to describe the other atoms that are not in the clusters.

In our method, we consider the atomic structure globally including 'glue' atoms, not only the atomic clusters. So, we choose the set B of large ASs as our starting point to ensure a reasonable atomic density. As already noticed, these large ASs already contain many high-symmetry orbits (see Fig. 10*a*). We optimize their number by using the full AS T_8 on bc and thus removing the corresponding part on n exactly as in the case of *i*-AlMnSi. The resulting model is shown in Fig. 13. The model has a composition of $Cd_{0.8942}RE_{10.58}$ and a density of 4.80 g cm^{-3} for RE = Gd. The RE atoms are distributed on a network of large icosahedra exactly like the Mn atoms in *i*-AlMnSi and *i*-AlPdMn since the chemical decoration of the node n is identical to that of the previous example of *i*-AlMnSi. This starting model, of course, like the preceding one of *i*-AlMnSi, shall certainly require substantial refinement to compare properly to the real structures; but all the basic ingredients are there, including the 'glue' atoms.

5. Conclusion

N-dimensional crystallography has proven to be a very natural and efficient tool to decipher the atomic structures of quasicrystals. Because it is based on the very definition of quasiperiodicity, the ideal models it generates are perfectly quasiperiodic and cannot as such properly represent the real objects. They should be considered as plausible initial perfect models for starting refinements using experimental data.

We have seen that one of the major features of having ASs located at special points in six dimensions is the existence in the structure of high-symmetry atomic clusters. This allowed us to focus our strategy on two simple goals: searching for maximum density together with the maximum number of complete orbits of large highly symmetric atomic clusters. These rules lead to a surprisingly small number of possibilities for each structure as demonstrated by the two examples of

i-AlMnSi with set *A* of global ASs and *i*-CdRE (RE = Gd, Ho, Tm) with set *B* for global ASs.

APPENDIX *A*
Diffraction pattern

Diffraction calculations are obtained by explicitly writing the Fourier transform of the density distribution obtained by the cut algorithm: the carrier of the Fourier spectrum is the $\mathbb{Z}$-module obtained by the projection of Λ^* in $\mathbf{E}_\parallel^*$: it is a *dense enumerable set of Bragg peaks*. The diffracted amplitude associated with a reflection $q = (q_\parallel, q_\perp) \in \mathbf{\Lambda}^*$ is given by

$$F(q_\parallel) = \sum_j f_j(q_\parallel)\widetilde{\eta}_j(q_\perp)\exp(2i\pi q \cdot r_j) \qquad (12)$$

where j runs over the ASs in the n-dimensional unit cell that defines the quasicrystal, $f_j(q_\parallel)$ is the atomic form factor of the atom j, $\widetilde{\eta}_j(q_\perp)$ the Fourier transform along $\mathbf{E}_\perp$ of the characteristic function of the jth AS and r_j its location in $\mathbf{E}^n$. This equation is identical to the usual expression in standard crystallography but with the additional $\widetilde{\eta}_j(q_\perp)$ term that is intrinsic to quasiperiodicity.

A few simple formulae allow us to easily compute the diffraction patterns associated with atomic clusters.

First of all, let T_1 and T_2 be two homothetic ASs in $\mathbf{E}_\perp$ with $T_2 = \beta T_1$ where β is the linear ratio between T_1 and T_2 so that for the volumes $V_{T_2} = \beta^3 V_{T_1}$. Let $\hat{\eta}_1(q_\perp)$ be the Fourier transform of the characteristic function $\eta_1(r_\perp)$ of T_1 that takes the value 1 inside T_1 and zero outside in $\mathbf{E}_\perp$:

$$\hat{\eta}_1(q_\perp) = \int_{r_\perp \in T_1} \exp(2i\pi q_\perp \cdot r_\perp)\,\mathrm{d}^3 r_\perp. \qquad (13)$$

The Fourier transform $\hat{\eta}_2(q_\perp)$ is obtained by noticing that $q_\perp \cdot r_\perp = \beta^{-1} q_\perp \cdot \beta r_\perp$ so that

$$\hat{\eta}_2(\beta^{-1} q_\perp) = \beta^3 \hat{\eta}_1(q_\perp). \qquad (14)$$

The calculation of the diffraction amplitudes associated with the atomic clusters is particularly simple in the case where the ASs $T_0(\widehat{\pi}_\perp t_j^k)$ in equation (11) have *no* intersections:

$$\widehat{\mathrm{AS}}_{\mathrm{AC}}(q_\parallel, q_\perp) = \hat{\eta}_0(q_\perp)\sum_{j=1}^{N} f_j(q_\parallel)\sum_{k=1}^{M_j}\exp(2i\pi q_\parallel \cdot t_{j\parallel}^k) \qquad (15)$$

where $f_j(q_\parallel)$ are the atomic form factors of the chemical species j.

For the case where the ASs $T_0(\widehat{\pi}_\perp t_j^k)$ have non-empty intersections, the calculation is slightly more complicated. Observing that the characteristic function of the intersection between two polyhedra T_1 and T_2 is the product $\eta_1(r_\perp)\eta_2(r_\perp)$, the Fourier transform of the union of the two polyhedra is written:

$$\widehat{\eta}_{T_1 \cup T_2}(q) = \widehat{\eta}_1(q) + \widehat{\eta}_2(q) - \sum_{q' \in \Lambda^*} \widehat{\eta}_1(q - q')\widehat{\eta}_2(q') \qquad (16)$$

so that

$$\widehat{\eta}_{T_1 \cup \ldots \cup T_N}(q) = \widehat{\eta}_{T_1 \cup \ldots \cup T_{N-1}}(q) + \widehat{\eta_N}(q) - \sum_{q' \in \Lambda^*} \widehat{\eta}_{T_1 \cup \ldots \cup T_{N-1}}(q - q')\widehat{\eta_N}(q'). \qquad (17)$$

This recurrent formula allows the explicit calculation of the diffraction amplitude [equation (15)] for overlapping ASs.

References

Arnol'd, V. I. (1988). *Physica D*, **33**, 21–25.
Besicovitch, A. S. (1932). *Almost Periodic Functions.* Cambridge University Press.
Bohr, H. (1924). *Acta Math.* **45**, 29–56.
Bohr, H. (1925). *Acta Math.* **46**, 101–123.
Bohr, H. (1926). *Acta Math.* **47**, 237–254.
Cahn, J. W., Gratias, D. & Mozer, B. (1988). *Phys. Rev. B*, **38**, 1638–1642.
Cahn, J. W., Shechtman, D. & Gratias, D. (1986). *J. Mater. Res.* **1**, 13–26.
Cooper, M. & Robinson, K. (1966). *Acta Cryst.* **20**, 614–617.
Duneau, M. & Oguey, C. (1989). *J. Phys. Fr.* **50**, 135–146.
Elser, V. (1996). *Philos. Mag. B*, **73**, 641–656.
Esclangon, E. (1904). Thèse à la faculté des sciences de Paris: Fonctions quasipériodiques.
Goldman, A. I., Kong, T., Kreyssig, A., Jesche, A. Ramazanoglu, M., Dennis, K. W. Bud'ko, S. L. & Canfield, P. C. (2013). *Nat. Mater.* **12**, 714–718.
Gratias, D., Cahn, J. W., Bessiere, M., Calvayrac, Y., Lefebvre, S., Quivy, A. & Mozer, B. (1987). *NATO Adv. Res. Workshop*, Acquafredda, October 1987.
Gummelt, P. (1996). *Geom. Dedicata*, **62**, 1–17.
Henley, C. L. (1986). *Phys. Rev. B*, **34**, 797–816.
Henley, C. L., de Boissieu, M. & Steurer, W. (2006). *Philos. Mag.* **86**, 1131–1151.
Janner, A. & Janssen, T. (1977). *Phys. Rev. B*, **15**, 643–658.
Kramer, P. (1988). *J. Math. Phys.* **29**, 516–527.
Levine, D. & Steinhardt, P. J. (1984). *Phys. Rev. Lett.* **53**, 2477–2480.
Oguey, C., Duneau, M. & Katz, A. (1988). *Commun. Math. Phys.* **118**, 99–118.
Shechtman, D. & Blech, I. (1985). *Metall. Trans. A*, **16**, 1005–1012.
Shechtman, D., Blech, I., Gratias, D. & Cahn, J. W. (1984). *Phys. Rev. Lett.* **53**, 1951–1953.
Steurer, W. (2006). *Philos. Mag.* **86**, 1105–1113.
Steurer, W. & Deloudi, S. (2012). *Struct. Chem.* **23**, 1115–1120.
Takakura, H., Yamamoto, A., de Boissieu, M. & Tsai, A. P. (2004). *Ferroelectrics*, **305**, 209–212.
Tsai, A. P., Guo, J. Q., Abe, E., Takakura, H. & Sato, T. J. (2000). *Nature (London)*, **408**, 537–538.